Rethinking Linear Modulation Range of Modular Multilevel Converters

Jingwei Meng, Qiang Song, *Senior Member, IEEE*, Qianhao Sun, Shukai Xu, *Senior Member, IEEE*, Biao Zhao, *Senior Member, IEEE*, Zhanqing Yu, *Member, IEEE*, and Rong Zeng, *Senior Member, IEEE*

***Abstract*—The linear modulation problem of modular multilevel converter (MMC) is considerably complicated by capacitor voltage ripples (CVRs) and circulating current suppression control (CCSC). This article examines the linear modulation range of MMC and its influence on parameter design and operating characteristics, taking into account the CVR effect and CCSC. The deviation between the actual voltage output and the reference is revealed and analyzed, and the analytical expression of this deviation is determined. The effects of CCSC on linear modulation are also revealed. Based on the article, a set of equations are proposed to determine the exact reference wave while accounting for the CVR effect and CCSC and precisely assess linear modulation. Subsequently, the linear modulation range of MMC, which is defined as the maximum selectable valve-side voltage that can satisfy whole operating region linear modulation in this article, can be exactly determined. Furthermore, how the CVR effect and CCSC influence the linear modulation range, parameter design, and operating characteristics are analyzed using case studies. The proposed theory and method are also verified through simulation and experimental results.**

***Index Terms*—Capacitor voltage ripples (CVRs), circulating current suppression control (CCSC), energy storage requirement, linear modulating range, modular multilevel converter (MMC).**

I. Introduction

MODULAR multilevel converters (MMCs) are regarded as a promising technology that offers major advantages, such as ease of implementation of a high number of levels, excellent harmonic performance, and low loss [1], [2], [3]. This technology has become the most competitive solution for the voltage-source converter (VSC)-based high-voltage direct current transmission system [4], [5], [6]. Similar to conventional pulsewidth modulation (PWM)-based converters, the linear modulation constraint determines the ac voltage output capability of MMC for a given dc voltage and has a significant influence on the parameter design and operating characteristics. The methodology for determining the linear modulation range of MMC is typically regarded as identical to that of conventional converters. However, few existing studies have noticed that the unique problems of MMC, such as capacitor voltage ripples (CVRs) and circulating current suppression control (CCSC), complicate the linear modulation problem.

Significant power fluctuation exists in each arm of the MMC. Power fluctuations cause the variation of energy stored in each arm, resulting in CVRs in each submodule (SM) [7], [8]. The additional voltage stress on the devices in SMs is the most direct result of the CVRs. To limit the capacitor voltage peak within an acceptable level, the SM capacitance should be designed large enough, resulting in the capacitor accounting for a considerable proportion in the cost and volume of an SM [9]. Many research efforts have focused on reducing the SM capacitance through decreasing the energy variation in the arms to minimize the cost and volume [10], [11], [12].

Circulating current can also be seen as a result of the CVRs. The CVRs generate a second-harmonic ripple component in the sum of the voltages of the upper and lower arms, resulting in the well-known second-harmonic circulating current flowing among the three-phase arms. The CCSC schemes that can suppress the second-harmonic circulating current to zero have been extensively studied [13], [14]. Some research efforts have focused on minimizing the energy variation and CVRs by injecting the appropriate circulating current [15], [16].

However, the effects of CVRs on other aspects of characteristics, particularly on the ac voltage output capability of MMC, have yet to be well explored. The ac voltage output for the conventional two-level and three-level VSCs is converted from the common dc-link voltage that has minor low-frequency ripple components. However, the ac voltage output of MMC is intrinsically generated by the differential voltages of the upper and lower arm voltages, instead of directly being converted from the common dc-link voltage. Given that the CVRs have a considerable influence on the voltages across the arms, they will inevitably affect the ac voltage output. Yang et al. [17] and Ma et al. [18] considered the impact of the CVRs on the dynamic behavior of MMC in electromagnetic transient model, but the steady-state analysis of the influence of CVRs on the linear modulation range is not involved. Oates [19] proposed an optimization process for defining the values of the

Manuscript received 19 October 2022; revised 9 January 2023; accepted 11 February 2023. Date of publication 21 February 2023; date of current version 20 April 2023. This work was supported in part by the National Key R&D Program of China under Grant 2022YFB2405300, and in part by the National Natural Science Foundation of China under Grant 51977119. Recommended for publication by Associate Editor A. Yazdani. *(Corresponding author: Qiang Song.)*

Jingwei Meng, Qiang Song, Qianhao Sun, Biao Zhao, Zhanqing Yu, and Rong Zeng are with the Department of Electrical Engineering, Tsinghua University, Beijing 100084, China (e-mail: mengjw19@mails.tsinghua.edu.cn; songqiang@tsinghua.edu.cn; sxsunqianhao@163.com; zhao-biao@tsinghua.edu.cn; yzq@tsinghua.edu.cn; zengrong@tsinghua.edu.cn).

Shukai Xu is with the Innovation Department of China Southern Power Grid, Guanzhou 510000, China (e-mail: xusk@csg.cn).

Color versions of one or more figures in this article are available at https://doi.org/10.1109/TPEL.2023.3246501.

Digital Object Identifier 10.1109/TPEL.2023.3246501

principle parameters, such as the ac voltage, phase reactance, SM capacitor voltage, etc., for given performance. However, the detailed mechanism of the impact of the CVRs on ac-side voltage capability and linear modulation range is not concerned in [19]. Liu et al. [20] reported that the CVRs affect the dc component of the SM capacitor voltage, but the further influence on the ac-side voltage output is not considered. Song et al. [21] reported that the CVRs can improve the ac voltage capability under capacitive reactive power conditions when using indirect modulation, but how the CVRs influence the linear modulation range cannot be exactly determined because it is only limited to qualitative analysis. Furthermore, the direct modulation, which is widely used in the existing papers and projects [22], has not been examined.

It is commonly believed that CCSC can decrease the arm current, the loss, and the required SM capacitance because the second-harmonic circulating component is eliminated from the arm current. However, this conclusion is obtained on the premise that the selectable valve-side ac voltage is not affected by the CCSC. If the ac voltage output capability can be affected by the CCSC, then the selectable valve-side ac voltages will be different whether the CCSC is activated or not. Consequently, the rated fundamental-frequency ac current will also be different when the CCSC is activated or not. Few existing articles have noticed the correlation between the CCSC and the ac voltage output capability. Thus, the evaluation of the effect of the CSCC on the parameter design and operating characteristics remains imprecise.

The linear modulation range of MMC and its effect on the parameter design and operating characteristics are reconsidered in this article, taking into account the CVR effect and CCSC. The rest of this article is organized as follows. Section II briefly describes the complexity of the linear modulation problem of MMC caused by CVR effect and CCSC. Section III reveals and analyzes the deviation between the actual voltage output and the reference and determines the analytical expression of this deviation. The effects of CCSC on the linear modulation are also presented in this section. Then, based on the analysis, a set of equations are proposed to obtain the exact reference while accounting for the CVR effect and CCSC, providing a method to precisely assess linear modulation. In Section IV, the linear modulation range of MMC is defined by the maximum selectable valve-side voltage that can satisfy whole operating region linear modulation (WOR-LM). Furthermore, how the CVR effect and CCSC influence the linear modulation range, parameter design, and operating characteristics are analyzed using case studies. Section V presents the simulation and experiment results. Finally, Section VI discusses the conclusions.

II. Linear Modulation Problem of MMC

A. Required AC Voltage Output for a Given Operating Point

Fig. 1(a) shows the single-line diagram of an MMC, each arm of which consists of N series-connected SMs and an arm inductor. The dc-side of the MMC is connected to the dc lines with a rated voltage of U_{dcN}. The ac-side of the MMC is connected to the ac grid via an interface transformer. The required

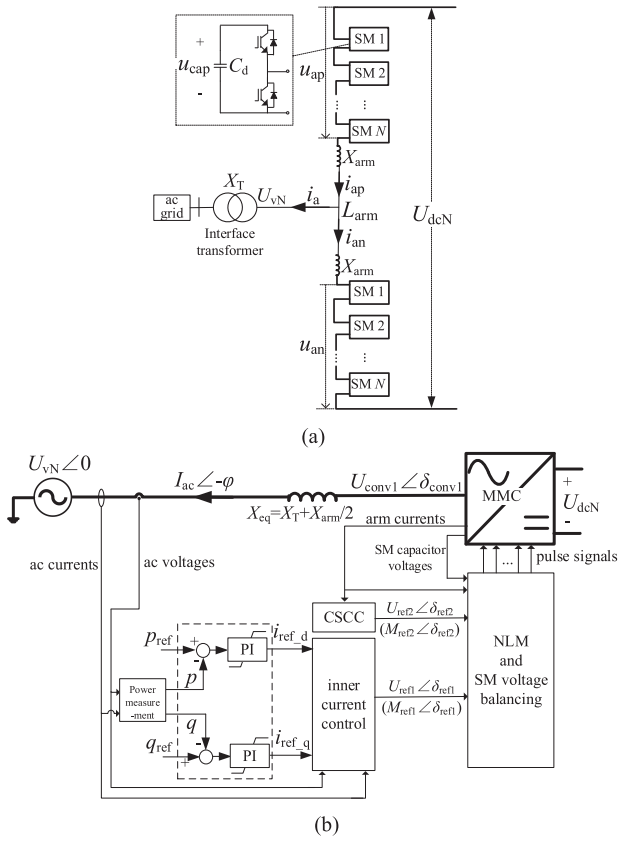

Fig. 1. Diagram of the MMC connected to an ac grid. (a) Single-line diagram of an MMC. (b) Equivalent circuit and the controller diagram.

amplitude of the ac voltage output should not exceed the ac voltage capability determined by linear modulation constraint for any possible operating point.

From the standpoint of the ac-side output, as illustrated in Fig. 1(b), the MMC is equivalent to being connected to an equivalent ac voltage source U_{vN} via an equivalent interface reactance X_{eq}, where U_{vN} is the rated valve-side voltage of the interface transformer and X_{eq} is determined by the leakage inductance of the interface transformer X_T and the arm inductance X_{arm} of the MMC. The active and reactive power are controlled through the fundamental-frequency ac voltage output $U_{\mathrm{conv1}}\angle\delta_{\mathrm{conv1}}$ of the MMC, which is equal to the sum of U_{vN} and the voltage drop across the equivalent inductance X_{eq}. When the MMC outputs a fundamental-frequency ac current $I_{\mathrm{ac}}\angle$-φ, the required fundamental-frequency ac voltage output U_{conv1} and δ_{conv1} can be expressed as follows:

$$U_{\mathrm{conv1}} = \sqrt{\left(U_{\mathrm{vN}} + X_{\mathrm{eq}} I_{\mathrm{ac}} \sin\varphi\right)^2 + \left(X_{\mathrm{eq}} I_{\mathrm{ac}} \cos\varphi\right)^2} \quad (1)$$

$$\delta_{\mathrm{conv1}} = \arctan\frac{X_{\mathrm{eq}} I_{\mathrm{ac}} \cos\varphi}{U_{\mathrm{vN}} + X_{\mathrm{eq}} I_{\mathrm{ac}} \sin\varphi}. \quad (2)$$

In (1), the required amplitude of the ac voltage output U_{conv1} is determined by the vale-side ac voltage U_{vN}, ac current output $I_{\mathrm{ac}}\angle$-φ, and inductance X_{eq}. For a given dc voltage, the amplitude of the ac voltage output is typically represented using the amplitude modulation index of the converter, which is defined

as the ratio of the amplitude of the line-to-ground ac voltage to half of the converter dc voltage

$$M_{\text{conv1}} = \frac{\sqrt{2}U_{\text{conv1}}}{U_{\text{dcN}}/2} = U^*_{\text{vN}}\sqrt{\left(1 + X^*_{\text{eq}}I^*_{\text{ac}}\sin\varphi\right)^2 + \left(X^*_{\text{eq}}I^*_{\text{ac}}\cos\varphi\right)^2} \quad (3)$$

where U^*_{vN} is the per-unit valve-side voltage normalized by $U_{\text{dcN}}/2$, I^*_{ac} is the per-unit ac current output, and X^*_{eq} is the per-unit equivalent interface reactance.

The linear modulation constraint determines the ac voltage output capability for a given dc voltage. The linear modulation condition is conventionally considered as $M_{\text{conv1}} \leq 1.0$ in case of no third-harmonic injection. However, the CVRs and the CCSC greatly complicate the linear modulation problem of MMC.

B. Complexity of the Linear Modulation Problem of MMC

Linear modulation is intrinsically determined by the magnitude ratio of the reference wave to the carrier wave. In particular, the linear modulation condition for the half-bridge SM based-MMC (HB-MMC) is that the insertion index for each arm is in the range of 0–*N*. Fig. 1(b) shows the general block diagram of the control system of MMCs, which mainly includes the outer-loop power controller, the inner-loop current controller, and the PWM. The outer-loop controller generates the *d*- and *q*-axis reference current. Then, the inner-loop current control generates the fundamental-frequency reference voltage $U_{\text{ref1}}\angle\delta_{\text{ref1}}$. The CCSC is optional and outputs the second-harmonic reference voltage $U_{\text{ref2}}\angle\delta_{\text{ref2}}$ for suppressing the second-harmonic circulating current. The reference voltages of the upper and lower arms for determining insertion indexes can be expressed as follows:

$$\begin{cases} u_{\text{ref\_ap}}(t) = \frac{U_{\text{dcN}}}{2} - \frac{\sqrt{2}U_{\text{ref1}}}{2}\sin(\omega t + \delta_{\text{ref1}}) \\ \quad + \frac{\sqrt{2}U_{\text{ref2}}}{2}\sin(2\omega t + \delta_{\text{ref2}}) \\ u_{\text{ref\_an}}(t) = \frac{U_{\text{dcN}}}{2} + \frac{\sqrt{2}U_{\text{ref1}}}{2}\sin(\omega t + \delta_{\text{ref1}}) \\ \quad + \frac{\sqrt{2}U_{\text{ref2}}}{2}\sin(2\omega t + \delta_{\text{ref2}}). \end{cases} \quad (4)$$

The nearest level modulation is the most widely used modulation scheme for MMCs. In existing studies and applications, the SM capacitor voltage is mainly regarded as its rated value when determining the number of inserted SMs in an arm [7], and it is expressed as follows:

$$U_{\text{capN}} = \frac{U_{\text{dcN}}}{N}. \quad (5)$$

Then, the insertion indexes for the upper and lower arm SMs are calculated as follows:

$$\begin{cases} n_{\text{ap}}(t) = \frac{u_{\text{ref\_ap}}(t)}{U_{\text{capN}}} \\ \quad = N\left[\frac{1}{2} - \frac{M_{\text{ref1}}}{2}\sin(\omega t + \delta_{\text{ref1}}) + \frac{M_{\text{ref2}}}{2}\sin(2\omega t + \delta_{\text{ref2}})\right] \\ n_{\text{an}}(t) = \frac{u_{\text{ref\_an}}(t)}{U_{\text{capN}}} \\ \quad = N\left[\frac{1}{2} + \frac{M_{\text{ref1}}}{2}\sin(\omega t + \delta_{\text{ref1}}) + \frac{M_{\text{ref2}}}{2}\sin(2\omega t + \delta_{\text{ref2}})\right] \end{cases} \quad (6)$$

where M_{ref1} and M_{ref2} are the magnitude ratios of the fundamental-frequency and second-harmonic reference waves, respectively, and they are expressed as follows:

$$M_{\text{ref1}} = \frac{\sqrt{2}U_{\text{ref1}}}{U_{\text{dcN}}/2} \quad (7)$$

$$M_{\text{ref2}} = \frac{\sqrt{2}U_{\text{ref2}}}{U_{\text{dcN}}/2}. \quad (8)$$

The ranges of values of M_{ref1} and M_{ref2} are restrained by linear modulation constraint. The criterion for judging the linear modulation for an HB-MMC is that the insertion index for the arm is in the range of 0–*N*, which can be expressed as follows:

$$0 \leq n_{\text{ap,n}} \leq N. \quad (9)$$

Considering the symmetry of the insertion indexes of the upper and lower arms shown in (6), linear modulation can be assessed by using the reference wave function defined as follows:

$$f_{\text{ref}}(t) = \frac{1}{2} + \frac{M_{\text{ref1}}}{2}\sin(\omega t + \delta_{\text{ref1}}) + \frac{M_{\text{ref2}}}{2}\sin(2\omega t + \delta_{\text{ref2}}). \quad (10)$$

Then, the linear modulation of an HB-MMC can be converted to the following constraint:

$$0 \leq f_{\text{ref}}(t) \leq 1. \quad (11)$$

The peak and valley values of the reference wave function in a fundamental-frequency period are denoted as f_{peak} and f_{valley}, respectively, and expressed as follows:

$$\begin{cases} f_{\text{peak}} = \max\left(f_{\text{ref}}(t)\right) \\ f_{\text{valley}} = \min\left(f_{\text{ref}}(t)\right) \end{cases} \quad 0 \leq t \leq T_1 \quad (12)$$

where T_1 is the fundamental-frequency period. The linear modulation constraint can also be expressed as follows:

$$f_{\text{peak}} \leq 1 \text{ and } f_{\text{valley}} \geq 0. \quad (13)$$

In (13), the upper and lower boundary constraints should be satisfied. To quantitatively evaluate the margin to the boundary constraints, the linear modulation margin Δf_{margin} is defined as the minimum of the upper and lower margins as follows:

$$\Delta f_{\text{margin}} = \min\left[\left(f_{\text{valley}} - 0\right), \left(1.0 - f_{\text{peak}}\right)\right]. \quad (14)$$

The linear modulation for a certain operating point is satisfied if Δf_{margin} is greater than zero. The lower the value of Δf_{margin}, the closer the MMC to the boundary condition of overmodulation.

Although (10)–(14) provide the expressions for assessing linear modulation, the manner by which to determine the exact values of M_{ref1}, δ_{ref1}, M_{ref2}, and δ_{ref2} is still a problem, which is reflected in the following aspects:

First, the fundamental-frequency reference $M_{\text{ref1}}\angle\delta_{\text{ref1}}$ in the PWM is conventionally considered to be equal to the required ac voltage output $M_{\text{conv1}}\angle\delta_{\text{conv1}}$. However, this article will reveal that this conventional view is invalid for MMC due to the existence of the CVRs and their effect on the ac voltage output. Specifically, the exact fundamental-frequency reference $M_{\text{ref1}}\angle\delta_{\text{ref1}}$ cannot be directly obtained for a given operating point by using the equivalent circuit shown in Fig. 1(b).

Second, the second-harmonic reference $M_{\text{ref2}}\angle\delta_{\text{ref2}}$ is injected when the CSCC is activated and influences the peak and

valley values of the reference wave function, which is rarely considered conventionally. According to the given operating point, the values of $M_{\text{ref2}}\angle\delta_{\text{ref2}}$ cannot be directly obtained either.

III. Impact Analysis of CVRs and CSCC on the AC Voltage Output and Reference Waves

This section discusses how to obtain the exact reference wave for a specific operating point while accounting for the CVR effect and CCSC to precisely access linear modulation of MMC.

A. CVR Effect Deviation Between the Actual AC Voltage Output and the Reference

1) Actual AC Voltage Output Considering the CVR Effect: Few existing MMC analyses and design methodologies consider the effects of CVRs when analyzing the fundamental-frequency ac voltage output, and it is simply expressed as

$$\begin{aligned} u_{\text{conv(ideal)}}(t) &= \frac{n_{\text{an}}(t)U_{\text{capN}} - n_{\text{ap}}(t)U_{\text{capN}}}{2} \\ &= M_{\text{ref1}}\frac{U_{\text{dcN}}}{2}\sin(\omega t+\delta_{\text{ref1}}). \end{aligned} \tag{15}$$

Specifically, the per-unit ac voltage output is regarded as the fundamental-frequency reference u^*_{ref1}

$$u^*_{\text{conv1(ideal)}}(t) = u^*_{\text{ref1}}(t) = M_{\text{ref1}}\sin(\omega t+\delta_{\text{ref1}}). \tag{16}$$

However, the existence of CVRs will deviate the actual ac voltage from the reference, which is defined as the CVR effect in this article. The CVR effect is reflected in two aspects. First, the CVRs affect the voltage across the arm through PWM, resulting in the generation of an additional ac component in the voltage output. This condition is the main deviation of the actual ac voltage from the reference. Second, the capacitor dc voltage does not always operate at its ideal value U_{capN} due to the CVR effect. Instead, the actual capacitor dc voltage must have a deviation from the rated value U_{capN} to counteract the CVR effect on the dc-side voltage, which has been reported in [20]. The deviation of the capacitor dc voltage from the rated value is also a cause of the deviation of the actual ac voltage output.

Instead of only accounting for the rated capacitor dc voltage, the CVR effect in each arm should also be considered, and the actual voltages across the upper and lower arms can be expressed as follows:

$$\begin{cases} u_{\text{ap}}(t) = n_{\text{ap}}(t)u_{\text{cap\_ap}}(t) \\ \quad = n_{\text{ap}}(t)\left(U_{\text{capN}} + \Delta\bar{U}_{\text{cap}} + \Delta\tilde{u}_{\text{cap\_ap}}(t)\right) \\ u_{\text{an}}(t) = n_{\text{ap}}(t)u_{\text{cap\_an}}(t) \\ \quad = n_{\text{an}}(t)\left(U_{\text{capN}} + \Delta\bar{U}_{\text{cap}} + \Delta\tilde{u}_{\text{cap\_an}}(t)\right) \end{cases} \tag{17}$$

where $\Delta\tilde{u}_{\text{cap\_ap}}$ and $\Delta\tilde{u}_{\text{cap\_an}}$ denote the CVRs in the upper and lower arms, respectively, and $\Delta\bar{U}_{\text{cap}}$ denotes the deviation component of the capacitor dc voltage relative to the rated value U_{capN}. It has been verified in [20] that the deviations of the capacitor dc voltage in the upper and lower arms are same.

The CVRs consist of multiple frequency components. When only considering the main frequency components, the CVRs can be expressed as follows:

$$\begin{cases} \Delta\tilde{u}_{\text{cap\_ap}}(t) = \Delta\tilde{u}_{\text{cap\_a(1)}}(t) + \Delta\tilde{u}_{\text{cap\_a(2)}}(t) \\ \quad + \Delta\tilde{u}_{\text{cap\_a(3)}}(t) \\ \Delta\tilde{u}_{\text{cap\_an}}(t) = -\Delta\tilde{u}_{\text{cap\_a(1)}}(t) + \Delta\tilde{u}_{\text{cap\_a(2)}}(t) \\ \quad - \Delta\tilde{u}_{\text{cap\_a(3)}}(t) \end{cases} \tag{18}$$

where $\Delta\tilde{u}_{\text{cap\_a(1)}}$, $\Delta\tilde{u}_{\text{cap\_a(2)}}$, and $\Delta\tilde{u}_{\text{cap\_a(3)}}$ are the fundamental-frequency, second-harmonic, and third-harmonic components, respectively. According to the steady-state model in [7], the detailed analytical expression of the CVRs are as follows:

$$\begin{aligned} \Delta\tilde{u}_{\text{cap\_a(1)}}(t) = {} & \frac{\sqrt{2}M^2_{\text{ref1}}I_{\text{ac}}}{8\omega C_{\text{d}}}\cos(\varphi+\delta_{\text{ref1}})\cos(\omega t+\delta_{\text{ref1}}) \\ & -\frac{\sqrt{2}I_{\text{ac}}}{4\omega C_{\text{d}}}\cos(\omega t-\varphi) - \frac{\sqrt{2}M_{\text{ref1}}k_{\text{cir}}I_{\text{ac}}}{4\omega C_{\text{d}}}\sin \\ & \times(\omega t+\theta_{\text{cir}}-\delta_{\text{ref1}}) \\ & +\frac{\sqrt{2}M_{\text{ref2}}I_{\text{ac}}}{8\omega C_{\text{d}}}\sin(\omega t+\delta_{\text{ref2}}+\varphi) \end{aligned} \tag{19}$$

$$\begin{aligned} \Delta\tilde{u}_{\text{cap\_a(2)}}(t) = {} & -\frac{\sqrt{2}M_{\text{ref1}}M_{\text{ref2}}I_{\text{ac}}}{16\omega C_{\text{d}}}\cos(\delta_{\text{ref1}}+\varphi)\cos \\ & \times(2\omega t+\delta_{\text{ref2}}) \\ & -\frac{\sqrt{2}k_{\text{cir}}I_{\text{ac}}}{4\omega C_{\text{d}}}\cos(2\omega t+\theta_{\text{cir}}) + \frac{\sqrt{2}M_{\text{ref1}}I_{\text{ac}}}{16\omega C_{\text{d}}}\sin \\ & \times(2\omega t+\delta_{\text{ref1}}-\varphi) \end{aligned} \tag{20}$$

$$\begin{aligned} \Delta\tilde{u}_{\text{cap\_a(3)}}(t) = {} & -\frac{\sqrt{2}M_{\text{ref1}}k_{\text{cir}}I_{\text{ac}}}{12\omega C_{\text{d}}}\sin(3\omega t+\delta_{\text{ref1}}+\theta_{\text{cir}}) \\ & -\frac{\sqrt{2}M_{\text{ref2}}I_{\text{ac}}}{24\omega C_{\text{d}}}\sin(3\omega t+\delta_{\text{ref2}}-\varphi) \end{aligned} \tag{21}$$

where C_{d} is the SM capacitance and k_{cir} is the amplitude index of the second-harmonic circulating current expressed as

$$k_{\text{cir}} = \frac{I_{\text{cir}}}{I_{\text{ac}}} \tag{22}$$

where I_{cir} and θ_{cir} are the rms value and phase of the second-harmonic circulating current, respectively. If the CCSC is inactive (i.e., $M_{\text{ref2}} = 0$), then the circulating currents will exist in the arms. The detailed expressions of I_{cir} and θ_{cir} are presented in Appendix. If the CCSC is applied, then the second-harmonic circulating current will be zero (i.e., $k_{\text{cir}} = 0$).

According to [20], the per-unit expression of the deviation of the capacitor voltage from the rated value can be deduced based on the CVR effect as follows:

$$\begin{aligned} \Delta\bar{U}^*_{\text{cap}} = {} & -4c_1M_{\text{ref1}}I^*_{\text{ac}}\sin(\varphi+\delta_{\text{ref1}}) \\ & -4c_1M^2_{\text{ref1}}k_{\text{cir}}I^*_{\text{ac}}\cos(\theta_{\text{cir}}-2\delta_{\text{ref1}}) \\ & +c_1M_{\text{ref1}}M_{\text{ref2}}I^*_{\text{ac}}\cos(\varphi+\delta_{\text{ref2}}-\delta_{\text{ref1}}). \end{aligned} \tag{23}$$

In contrast with the ideal expression shown in (15), the actual ac voltage output taking into account the CVR effect should be

expressed as follows:

$$u_{\text{conv}}(t) = \frac{u_{\text{an}}(t) - u_{\text{ap}}(t)}{2} = u_{\text{conv(ideal)}}(t) + \frac{n_{\text{an}}(t)\Delta\tilde{u}_{\text{cap\_an}}(t) - n_{\text{ap}}(t)\Delta\tilde{u}_{\text{cap\_ap}}(t)}{2} + \frac{n_{\text{an}}(t) - n_{\text{ap}}(t)}{2}\Delta\bar{U}_{\text{cap}}. \quad (24)$$

The second and third items on the right-hand side of (24) represent the ac voltage output components generated by the ac ripple and dc deviation components in the capacitor voltage, respectively. The main concern of this article is the fundamental-frequency voltage output, which is the fundamental-frequency component of (24). The next section will analyze in detail how the fundamental-frequency ac voltage output deviates from the ideal value due to the CVR effect.

2) Deviation Component Directly Caused by CVRs: First, the second item on the right-hand side of (24) represents the deviation component directly generated by CVRs. Items $n_{\text{ap}}(t)\Delta\tilde{u}_{\text{cap\_ap}}(t)$ and $n_{\text{an}}(t)\Delta\tilde{u}_{\text{cap\_an}}(t)$ contain fundamental-frequency ac components. Using $n_{\text{ap}}(t)\Delta\tilde{u}_{\text{cap\_ap}}(t)$ as an example, the functions $n_{\text{ap}}(t)$ and $\Delta\tilde{u}_{\text{cap\_ap}}(t)$ contain fundamental-frequency and second-harmonic ac components, respectively, as illustrated in (6) and (20). Thus, their product must generate a fundamental-frequency ac component, the per-unit value of which is denoted using $\Delta u^*_{\text{cvr\_1}}$.

The final expression of $\Delta u^*_{\text{cvr\_1}}$ can be obtained by substituting (6) and (19)–(21) into the second item on the right-hand side of (24) and then extracting the fundamental-frequency ac component

$$\begin{aligned}\Delta u^*_{\text{cvr\_1}}(t) &= c_1 I^*_{\text{ac}}(8 + M^2_{\text{ref1}})\sin(\varphi + \delta_{\text{ref1}})\sin(\omega t + \delta_{\text{ref1}}) \\ &+ c_1 I^*_{\text{ac}}(8 - 3M^2_{\text{ref1}})\cos(\varphi + \delta_{\text{ref1}})\cos(\omega t + \delta_{\text{ref1}}) \\ &+ 12c_1 M_{\text{ref1}} k_{\text{cir}} I^*_{\text{ac}} \sin(\omega t + \theta_{\text{cir}} - \delta_{\text{ref1}}) \\ &- c_1 M^2_{\text{ref1}} M_{\text{ref2}} I^*_{\text{ac}} \cos(\delta_{\text{ref1}} + \varphi)\sin(\omega t - \delta_{\text{ref1}} + \delta_{\text{ref2}}) \\ &- \frac{4c_1 M^2_{\text{ref2}} I^*_{\text{ac}}}{3}\cos(\omega t - \varphi) \end{aligned} \quad (25)$$

where c_1 is a constant coefficient determined by the MMC parameters, as illustrated in Appendix.

3) Deviation Component Caused by the DC Deviation of the Capacitor Voltage: The third item on the right-hand side of (24) represents the ac voltage component generated by the dc deviation of the capacitor voltage. The per-unit value of this deviation voltage in the ac voltage output is denoted using $\Delta u^*_{\text{cvr\_2}}$. The final expression of $\Delta u^*_{\text{cvr\_2}}$ can be obtained by substituting (6) and (23) into the third item on the right-hand side of (24) and extracting the fundamental-frequency ac component

$$\begin{aligned}\Delta u^*_{\text{cvr\_2}}(t) &= -4c_1 M^2_{\text{ref1}} I^*_{\text{ac}} \sin(\omega t + \delta_{\text{ref}})\sin(\varphi + \delta_{\text{ref1}}) \\ &- 4c_1 M^3_{\text{ref1}} k_{\text{cir}} I^*_{\text{ac}} \sin(\omega t + \delta_{\text{ref}})\cos(\theta_{\text{cir}} - 2\delta_{\text{ref1}}) \\ &+ c_1 M^2_{\text{ref1}} M_{\text{ref2}} I^*_{\text{ac}} \sin(\omega t + \delta_{\text{ref}})\cos(\varphi + \delta_{\text{ref2}} - \delta_{\text{ref1}}). \end{aligned} \quad (26)$$

4) Actual AC Voltage Output Considering the CVR Effect Deviations and an Example Analysis: The actual ac voltage output in per-unit can be expressed as follows:

$$u^*_{\text{conv1}}(t) = u^*_{\text{ref1}}(t) + \underbrace{\Delta u^*_{\text{cvr\_1}}(t) + \Delta u^*_{\text{cvr\_2}}(t)}_{\text{CVR effect deviation}} \quad (27)$$

where the total deviation of the ac voltage output from the reference caused by the CVR effect can be expressed in per-unit as follows:

$$\begin{aligned}\Delta u^*_{\text{cvr}}(t) &= \Delta u^*_{\text{cvr\_1}}(t) + \Delta u^*_{\text{cvr\_2}}(t) \\ &= \underbrace{c_1 I^*_{\text{ac}}(8 - 3M^2_{\text{ref1}})\sin(\varphi + \delta_{\text{ref1}})\sin(\omega t + \delta_{\text{ref1}})}_{\text{direct deviation}} \\ &+ \underbrace{c_1 I^*_{\text{ac}}(8 - 3M^2_{\text{ref1}})\cos(\varphi + \delta_{\text{ref1}})\cos(\omega t + \delta_{\text{ref1}})}_{\text{quadrature deviation}} \\ &+ 12c_1 M_{\text{ref1}} k_{\text{cir}} I^*_{\text{ac}} \sin(\omega t + \theta_{\text{cir}} - \delta_{\text{ref1}}) \\ &\underbrace{- 4c_1 M^3_{\text{ref1}} k_{\text{cir}} I^*_{\text{ac}} \cos(2\delta_{\text{ref1}} - \theta_{\text{cir}})\sin(\omega t + \delta_{\text{ref1}})}_{\text{related with second - harmonic circulating current}} \\ &\underbrace{c_1 I^*_{\text{ac}} M_{\text{ref2}}\left[-\frac{4M_{\text{ref2}}}{3} + M^2_{\text{ref1}}\sin(2\delta_{\text{ref1}} - \delta_{\text{ref2}})\right]\cos(\omega t - \varphi)}_{\text{related with CCSC}}. \end{aligned} \quad (28)$$

As illustrated in (28), Δu^*_{cvr} mainly contains direct and quadrature deviation components according to their phase relationship with the ideal value. It also contains a deviation component related with the second-harmonic component, and the influence of which is relatively minor because index k_{cir} or M_{ref2} is relatively small. The amplitudes of the direct and quadrature deviation components are mainly determined by power factor angle φ and ac current I^*_{ac} because the value of δ_{ref1} is small.

Fig. 2 shows the waveforms of the reference and the actual ac voltage output of an example MMC under several typical power factor angles, whereas I^*_{ac} is kept as 1.0 p.u. In this example, the CCSC is inactive and M_{ref2} is simply set as zero. In Fig. 2, the actual ac voltage output deviates from the reference because of the CVR effect for all operating conditions. However, the

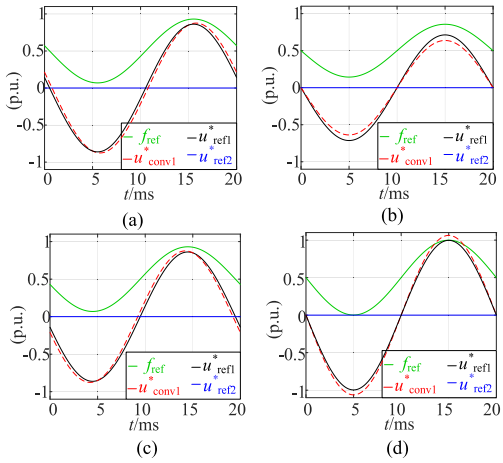

Fig. 2. Diagram of the waveforms of the reference and the actual output AC voltages when the CCSC is inactive. (a) $\varphi = -\pi$. (b) $\varphi = -\pi/2$. (c) $\varphi = 0$. (d) $\varphi = \pi/2$.

influences of the CVR effect deviation on the linear modulation vary with operating conditions.

When the MMC absorbs and outputs active power, as shown in Fig. 2(a) and (c), the quadrature deviation component exerts a significant effect on the voltage deviation, and the direct deviation component is minor. In these cases, the CVR deviation mainly causes a phase difference between the actual ac voltage output and the reference. The linear modulation is almost unaffected because the difference between the amplitudes of the actual ac voltage and the reference is minor.

When the MMC absorbs and outputs reactive power, as shown in Fig. 2(b) and (d), the direct deviation exerts a significant effect on the voltage deviation and mainly causes an amplitude difference between the actual ac voltage output and the reference. The effects on the amplitude under capacitive and inductive operating conditions are opposite. In Fig. 2(d), the MMC outputs an ac voltage with a higher amplitude than the reference when the reactive power is capacitive. However, the amplitude of the actual ac voltage is lower than the reference when the reactive power is inductive, as illustrated in Fig. 2(b).

In summary, the CVR effect causes a deviation between the amplitudes of the actual ac voltage output and the reference, affecting linear modulation. This effect becomes stronger with the increase in the power factor angle. Under capacitive operating conditions, the amplitude of the reference is lower than that of the ac voltage output, which is beneficial to linear modulation. Moreover, the reverse applies under inductive operating conditions. Overall, the CVR effect is advantageous in increasing the linear modulation range of MMC. Because for the whole operating region, the required higher ac voltage under capacitive operating conditions is the key constraint to linear modulation. In Fig. 2(d), the amplitude of ac voltage output can even exceed 1.0 due to the CVR effect deviation. But, the amplitude of the reference wave is still lower than 1.0, and the linear modulation condition is still satisfied.

B. Effect of CCSC on the Reference Wave and Linear Modulation

If CCSC is applied, then the second-harmonic component $M_{\mathrm{ref2}}\angle\delta_{\mathrm{ref2}}$ will exist in the reference wave and affect the linear modulation. The exact values of M_{ref2} and δ_{ref2} should be obtained to obtain the exact reference wave. The objective of CCSC is to suppress the second-harmonic circulating current to zero. According to the method presented in [15], the required amplitude and phase of the second-harmonic reference can be solved by the following equations:

$$\begin{cases} 6c_1 M_{\mathrm{ref1}} I_{\mathrm{ac}}^* \cos(\delta_{\mathrm{ref1}}-\varphi) - 2c_1 M_{\mathrm{ref1}}^3 I_{\mathrm{ac}}^* \cos(\varphi+\delta_{\mathrm{ref1}})\cos 2\delta_{\mathrm{ref1}} \\ \quad + M_{\mathrm{ref2}} \cos\delta_{\mathrm{ref2}} \bar{U}_{\mathrm{cap}}^* - \frac{2c_1 M_{\mathrm{ref1}} M_{\mathrm{ref2}} I_{\mathrm{ac}}^*}{3} \cos(\delta_{\mathrm{ref1}}+\varphi)\sin\delta_{\mathrm{ref2}} \\ \quad - \frac{4c_1 M_{\mathrm{ref1}} M_{\mathrm{ref2}} I_{\mathrm{ac}}^*}{3} \sin(\delta_{\mathrm{ref1}}+\varphi)\cos\delta_{\mathrm{ref2}} = 0 \\ 6c_1 M_{\mathrm{ref1}} I_{\mathrm{ac}}^* \sin(\delta_{\mathrm{ref1}}-\varphi) - 2c_1 M_{\mathrm{ref1}}^3 I_{\mathrm{ac}}^* \cos(\varphi+\delta_{\mathrm{ref1}})\sin 2\delta_{\mathrm{ref1}} \\ \quad + M_{\mathrm{ref2}} \sin\delta_{\mathrm{ref2}} \bar{U}_{\mathrm{cap}}^* + \frac{2c_1 M_{\mathrm{ref1}} M_{\mathrm{ref2}} I_{\mathrm{ac}}^*}{3} \cos(\delta_{\mathrm{ref1}}+\varphi)\cos\delta_{\mathrm{ref2}} \\ \quad - \frac{4c_1 M_{\mathrm{ref1}} M_{\mathrm{ref2}} I_{\mathrm{ac}}^*}{3} \sin(\delta_{\mathrm{ref1}}+\varphi)\sin\delta_{\mathrm{ref2}} = 0. \end{cases} \tag{29}$$

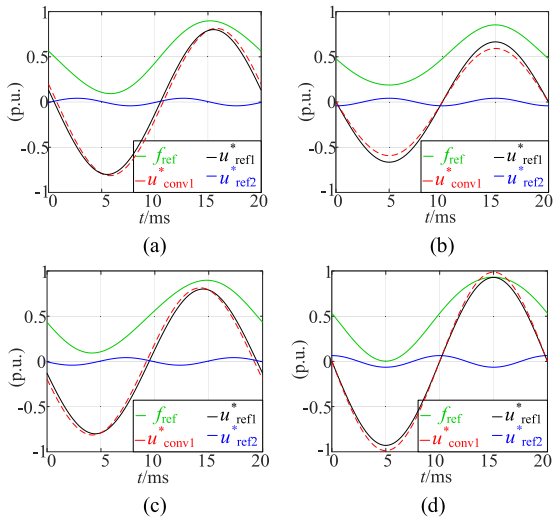

Fig. 3. Diagram of the waveforms of the reference and the actual output AC voltages when the CCSC is active. (a) $\varphi = -\pi$. (b) $\varphi = -\pi/2$. (c) $\varphi = 0$. (d) $\varphi = \pi/2$.

When the CCSC is applied in the abovementioned example MMC, Fig. 3 shows the waveforms of the fundamental-frequency reference, the second-harmonic reference, and the actual ac voltage output under several typical power factor angles, whereas I_{ac}^* is kept as 1.0 p.u.

Similar to the waveforms shown in Fig. 2, the deviation between the actual ac voltage output and the reference wave can still be observed for all operating conditions when the CCSC is applied. Given that the second-harmonic reference of the upper and lower arms are identical, they do not directly affect the differential ac voltage output. Although the expression of the CVR effect deviations shown in (28) contains the items of M_{ref2} and δ_{ref2}, the effect of the second-harmonic reference on the CVR effect deviation is minor because M_{ref2} is always small.

However, the second-harmonic component that is injected into the reference wave directly affects the peak and valley values of the reference wave function $f_{\mathrm{ref}}(t)$, resulting in a significant influence on linear modulation. Fig. 3 also illustrates the different effects under the various power factor angles.

When the MMC absorbs and outputs active power, as shown in Fig. 3(a) and (c), the peak and valley of the fundamental-frequency reference correspond with the zero point of the second-harmonic reference. Accordingly, the second-harmonic reference has a minor influence on the peak and valley values f_{peak} and f_{valley} of the reference wave function and a minor influence on linear modulation. However, the situation is different when the MMC outputs or absorbs reactive power.

At the rated capacitive reactive power point ($\varphi = \pi/2$), as shown in Fig. 3(d), the peak and valley of the fundamental-frequency reference correspond with the valley of the second-harmonic reference. Therefore, the second-harmonic reference plays a role in moving the reference wave function waveform downward, making f_{valley} closer to the lower limit and f_{peak} farther from the upper limit.

At the rated inductive reactive power point ($\varphi = -\pi/2$), as shown in Fig. 3(b), the peak and valley of the fundamental-frequency reference correspond with the peak of

the second-harmonic reference. Therefore, the second-harmonic reference plays a role in moving the reference wave function waveform upward, making f_{peak} closer to the upper limit and f_{valley} farther from the lower limit.

The second-harmonic component breaks the symmetry of the reference wave function $f_{\text{ref}}(t)$ relative to the upper and lower boundaries and reduces the linear modulation margin Δf_{margin}. From this point of view, the second-harmonic reference generated by CCSC is unfavorable to linear modulation. This phenomenon is more evident in the capacitive reactive power region because the required ac voltage output is higher in this region and the linear modulation margin is lower. The decreased value of f_{valley} caused by the second-harmonic reference makes it more likely to break the lower boundary constraint for linear modulation in this region.

C. 4-D Nonlinear Equations for Solving the Exact Reference for a Given Operating Point

The key to assessing the linear modulation for a given operating point is how to obtain the exact values of M_{ref1}, δ_{ref1}, M_{ref2}, and δ_{ref2} for calculating f_{peak} and f_{valley}. According to the above-presented analytical model considering the CVR effect and CCSC, a set of four-dimensional (4-D) simultaneous equations is proposed to solve the exact values of M_{ref1}, δ_{ref1}, M_{ref2}, and δ_{ref2} in this article.

As shown in the equivalent circuit in Fig. 1(b), the required ac voltage output $M_{\text{conv1}}\angle\delta_{\text{conv1}}$ for a given operating point (i.e., for the given active and reactive power) is certain and can be directly obtained using (1)–(3). In this article, deviation occurred between the actual ac voltage output and the reference. Accordingly, the reference wave must be adjusted to ensure that the actual ac voltage output shown in (27) is equal to the required ac voltage output $M_{\text{conv1}}\angle\delta_{\text{conv1}}$. If these two phasors are equal, the real and imaginary parts of the two phasors should be equal, respectively [23], [24]. Then, the following equations can be obtained by substituting (28) into (27):

$$\begin{cases} M_{\text{conv1}}\cos\delta_{\text{conv1}} = M_{\text{ref1}}\cos\delta_{\text{ref1}} + 12c_1M_{\text{ref1}}k_{\text{cir}}I_{\text{ac}}^*\cos(\theta_{\text{cir}}-\delta_{\text{ref1}}) \\ +c_1I_{\text{ac}}^*(8-3M_{\text{ref1}}^2)\sin(\varphi+\delta_{\text{ref1}})\cos\delta_{\text{ref1}} \\ -c_1I_{\text{ac}}^*(8-3M_{\text{ref1}}^2)\cos(\varphi+\delta_{\text{ref1}})\sin\delta_{\text{ref1}} \\ -4c_1M_{\text{ref1}}^3k_{\text{cir}}I_{\text{ac}}^*\cos(2\delta_{\text{ref1}}-\theta_{\text{cir}})\cos\delta_{\text{ref1}} \\ +c_1I_{\text{ac}}^*M_{\text{ref2}}\left[-\frac{4M_{\text{ref2}}}{3}+M_{\text{ref1}}^2\sin(2\delta_{\text{ref1}}-\delta_{\text{ref2}})\right]\sin\varphi \\ M_{\text{conv1}}\sin\delta_{\text{conv1}} = M_{\text{ref1}}\sin\delta_{\text{ref1}} + 12c_1M_{\text{ref1}}k_{\text{cir}}I_{\text{ac}}^*\sin(\theta_{\text{cir}}-\delta_{\text{ref1}}) \\ +c_1I_{\text{ac}}^*(8-3M_{\text{ref1}}^2)\sin(\varphi+\delta_{\text{ref1}})\sin\delta_{\text{ref1}} \\ +c_1I_{\text{ac}}^*(8-3M_{\text{ref1}}^2)\cos(\varphi+\delta_{\text{ref1}})\cos\delta_{\text{ref1}} \\ -4c_1M_{\text{ref1}}^3k_{\text{cir}}I_{\text{ac}}^*\cos(2\delta_{\text{ref1}}-\theta_{\text{cir}})\sin\delta_{\text{ref1}} \\ +c_1I_{\text{ac}}^*M_{\text{ref2}}\left[-\frac{4M_{\text{ref2}}}{3}+M_{\text{ref1}}^2\sin(2\delta_{\text{ref1}}-\delta_{\text{ref2}})\right]\cos\varphi \end{cases} \tag{30}$$

M_{ref1}, δ_{ref1}, M_{ref2}, and δ_{ref2} are the four unknown variables to be solved in (30). Another two equations are needed to solve these four unknown variables. Equation (29) describes the required values of M_{ref2} and δ_{ref2} when using CCSC. Accordingly, (29) and (30) can form a simultaneous 4-D nonlinear equations.

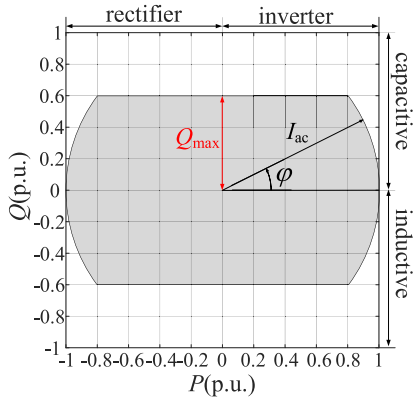

Fig. 4. PQ diagram of MMC.

In any given operating point, the exact values of M_{ref1}, δ_{ref1}, M_{ref2}, and δ_{ref2} can be obtained by solving the 4-D nonlinear equations. Then, f_{peak} and f_{valley} can be calculated, and the linear modulation of this operating point can be judged according to (12) and (13).

IV. Linear Modulation Range and Its Effects on the Parameter Design and Operating Characteristics

A. WOR-LM

A key design consideration of the parameters of the MMC is that all possible operating points should satisfy linear modulation. The operating region of MMC can be described using the PQ diagram, as shown in Fig. 4. The figure demonstrates that the active and reactive power are expressed in per-unit normalized by the rated active power. In real applications, the required reactive power capability needs not be extremely high as the rated active power. Accordingly, the maximum reactive power of the PQ diagram, which is denoted using $Q_{\max}$, can vary according to the grid requirement. WOR-LM is defined in this article as all operating points within the whole operating region satisfying linear modulation.

Based on the proposed linear modulation judging method for each operating point, all the operating points along the boundary of the PQ diagram can be scanned to check whether WOR-LM is satisfied for the designed parameters. The flowchart for judging WOR-LM is shown in Fig. 5. First, the designed parameters are inputted, and the initial value of power factor angle φ is set as $-\pi$. Then, the power factor angle φ varies from $-\pi$ to π step by step, while the per-unit ac current is set as the corresponding value on the boundary of the PQ diagram.

At each scanned operating point, the required ac voltage output $M_{\text{conv1}}\angle\delta_{\text{conv1}}$ can be obtained using (1)–(3). Then, the corresponding exact values of M_{ref1}, δ_{ref1}, M_{ref2}, and δ_{ref2} can be solved by using the 4-D nonlinear equations formed by (29) and (30). The solved values of M_{ref1}, δ_{ref1}, M_{ref2}, and δ_{ref2f} can be substituted into (10) to obtain the reference wave function $f_{\text{ref}}(t)$. Then, f_{peak} and f_{valley} can be obtained using (12). Subsequently, the linear modulation of this operating point can be judged using (13). Furthermore, the linear modulation margin Δf_{margin} can

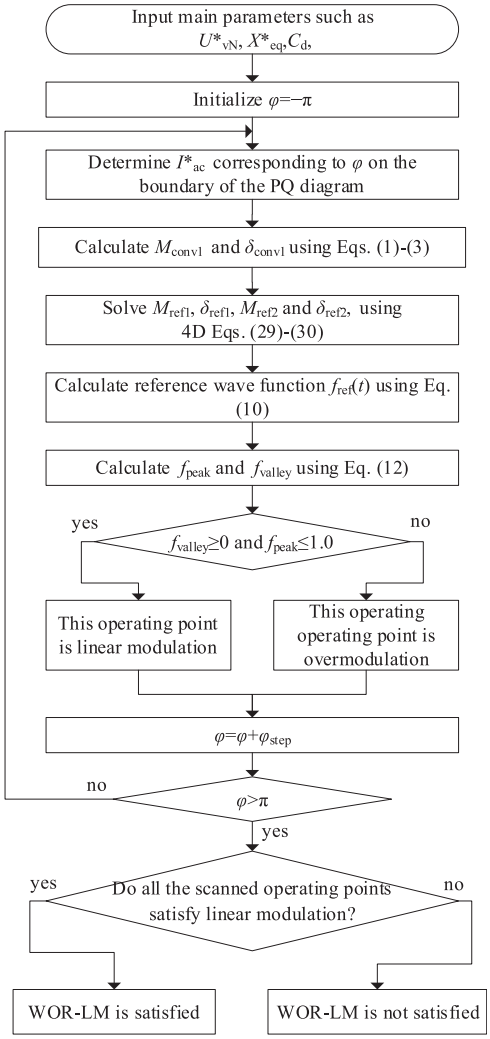

Fig. 5. Flowchart for judging WOR-LM.

TABLE I
KEY PARAMETERS OF THE SIMULATION MODEL

Item	Value
Rated active power P_N	1250 MW
Rated dc-link voltage U_{dcN}	400 kV
Number of SMs in an arm N	200
Rated SM capacitor voltage U_{capN}	2000 V
Upper limit of the capacitor voltage peak ε_{lim}	1.1 p.u.
Equivalent interface inductance X^*_{eq}	0.25 p.u.
Arm inductance (converted to the valve-side) $X_{arm}{}^*$	0.15 p.u.
Leakage inductance of the interface transformer $X_T{}^*$	0.10 p.u

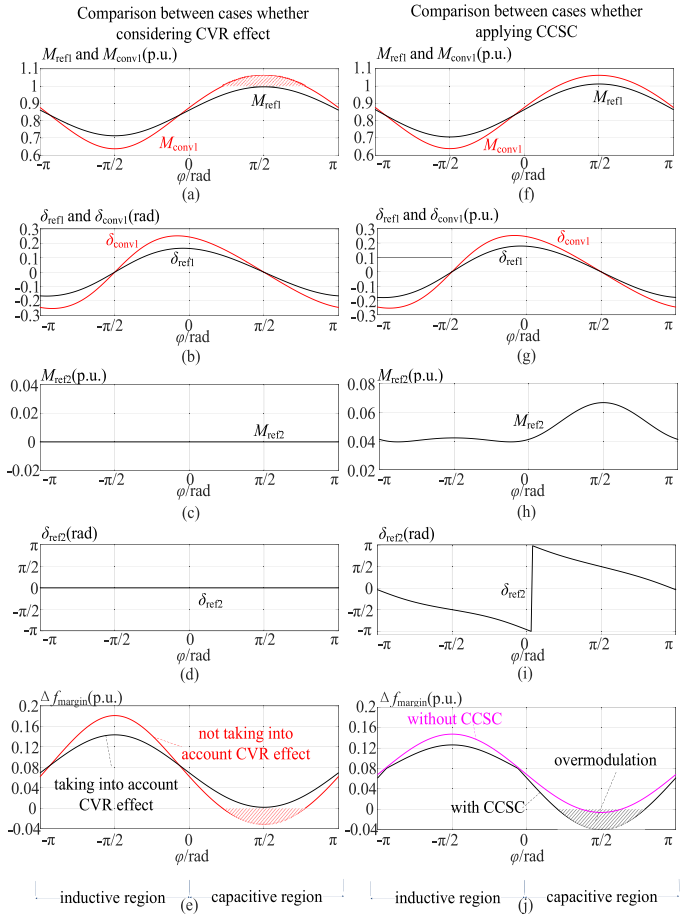

Fig. 6. Curves of the analysis results using the proposed judging method for WOR-LM.

also be obtained using (14) to assess the risk of overmodulation at this operating point.

After all the operating points on the boundary of the PQ diagram are scanned, the availability of the designed parameters can be judged from the standpoint of WOR-LM. If all the scanned operating points satisfy linear modulation, then the designed parameters can satisfy the WOR-LM constraint. Otherwise, the parameters need to be optimized until WOR-LM is satisfied.

A case study is used to demonstrate how the CVR effect and CCSC influence WOR-LM. The main parameters of the case study are listed in Table I, and the value of Q_{max} of the PQ diagram is set as 1.0 p.u. Fig. 6 shows the curves of the analysis results using the proposed judging method for WOR-LM. The cases with and without of CCSC are both studied.

Fig. 6(a)–(e) (left column) show the analysis results of the case when the CCSC is inactive. Fig. 6(a) compares the curves of the reference amplitude M_{ref1} and the actual ac voltage amplitude M_{conv1} following the change of power factor angel φ along the boundary of the given PQ diagram. Reference amplitude M_{ref1} differs from the actual ac output voltage M_{conv1} because of the CVR effect, and the deviation degree varies with the operating conditions. In the inductive operating region (i.e., when φ ranges from $-\pi$ to zero) shown in Fig. 6(a), the reference amplitude M_{ref1} is higher than the actual ac voltage M_{conv1}, and the maximum deviation occurs at the rated inductive reactive power point ($\varphi = -\pi/2$). In the capacitive operating region (when φ ranges from zero to π) shown in Fig. 6(a), reference amplitude M_{ref1} is lower than the actual ac output voltage M_{conv1} and the maximum deviation occurs at the rated capacitive reactive power point ($\varphi = \pi/2$).

Although the CVRs have opposing effects on the reference amplitude in the capacitive and inductive regions, the CVR effect is overall advantageous to WOR-LM because the required ac voltage is higher in the capacitive region, whereas the CVR effect

plays a role in decreasing the reference amplitude in this region. This condition can also be observed from the curves of the linear modulation margin shown in Fig. 6(e). In Fig. 6(e), a negative region appears when the conventional method is used without considering the CVR effect (i.e., M_{ref1} is ideally considered to be M_{conv1}), indicating conservative judgment of overmodulation, and the valve-side voltage has to be decreased, which results in an uneconomical design of the MMC parameters and brings an unnecessary increase in the cost and size. The proposed method taking into account the CVR effect can obtain the accurate result for judging WOR-LM and helps in selecting more reasonable parameters.

Fig. 6(f)–(j) (right column) show the analysis results of the case when the CCSC is active. The curves of the amplitude and phase of the injected second-harmonic reference following the change of the operating points are shown in Fig. 6(h) and (i). The conclusion about the influence of the CVR effect is similar to that of the case without CCSC. Specifically, taking into consideration the CVR effect can yield an accurate linear modulation margin that is larger than that obtained using the conventional method that does not take into account the CVR effect.

The results illustrated in Fig. 6(j) also verify the conclusion of the effect of CSCC on linear modulation. The comparison results of the curves shown in Fig. 6(j) indicate that the linear modulation margin is decreased when the CCSC is applied. This finding indicates that the application of CCSC renders the MMC susceptible to overmodulation, which is consistent with the analysis presented in Section III-B.

B. Linear Modulation Range Defined by the Maximum Selectable Valve-Side Voltage

The selection of the valve-side voltage of the interface transformer U^*_{vN} is critical from the standpoint of WOR-LM. A lower valve-side voltage U^*_{vN} is beneficial to satisfy WOR-LM because the required converter ac voltage output is equal to the sum of the valve-side voltage and the voltage drop across the equivalent interface inductance. However, a higher valve-side voltage is preferable in terms of minimizing the arm current, loss, and SM capacitance [19]. Accordingly, the rated valve-side voltage U^*_{vN} for a given rated dc-side voltage and PQ diagram can be selected as high as possible under the premise that WOR-LM is satisfied. This article proposes to use the maximum selectable valve-side voltage to define the linear modulation range of an MMC. The linear modulation range $U^*_{\mathrm{vN\_LMR}}$ is defined as the maximum per-unit valve-side voltage under which WOR-LM can be satisfied.

Based on the proposed WOR-LM judging method, the flowchart for determining the linear modulation range $U^*_{\mathrm{vN\_LMR}}$ for a given PQ diagram is shown in Fig. 7. The linear modulation range is highly correlated to the maximum reactive power capability $Q_{\max}$ and the equivalent interface reactance X_{eq} because the reactive current generates the voltage drop across the equivalent interface reactor. Accordingly, the linear modulation range $U^*_{\mathrm{vN\_LMR}}$ is searched for the given values of $Q_{\max}$ and X_{eq}. First, U^*_{vN} can be initialized to a low value. Subsequently, WOR-LM is checked for this value of U^*_{vN} using the flowchart

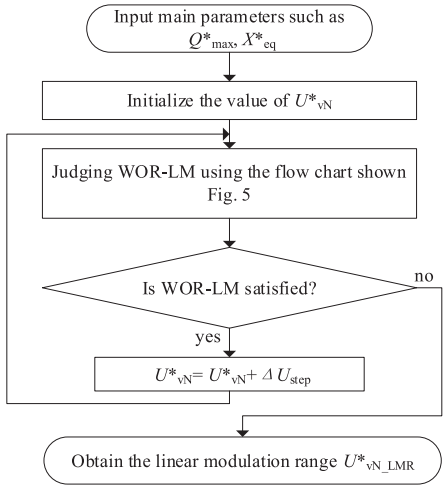

Fig. 7. Flowchart for searching the linear modulation range $U^*_{\mathrm{vN\_LMR}}$.

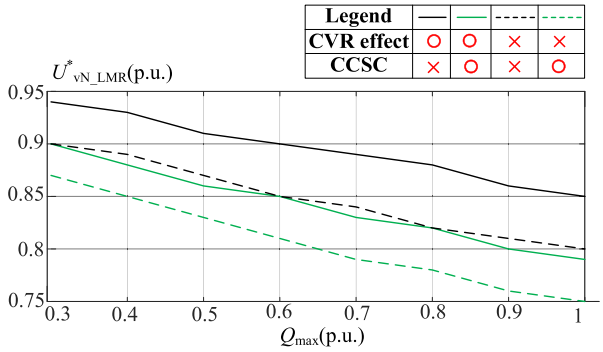

Fig. 8. Curves of the linear modulation range following the change of $Q_{\max}$ for the various cases.

shown in Fig. 5. If WOR-LM is satisfied, then a higher value U^*_{vN} is possible, and U^*_{vN} is increased by a step to check the WOR-LM again. The process is repeated until U^*_{vN} is increased to a value that cannot satisfy WOR-LM. Thereafter, the linear modulation range $U^*_{\mathrm{vN\_LMR}}$ can be determined as the maximum U^*_{vN} that can satisfy WOR-LM.

Fig. 8 illustrates the curves of the calculated results of the linear modulation range $U^*_{\mathrm{vN\_LMR}}$ following the change of $Q_{\max}$ under various cases, such as whether the CVR effect is taken into account and whether CCSC is applied, whereas X_{eq} is set as 0.25 p.u.

In each case, the linear modulation range $U^*_{\mathrm{vN\_LMR}}$ decreases with the increase in $Q_{\max}$ because the higher capacitive reactive power requirement increases the required amplitude of the ac voltage output. Therefore, a reasonable setting of the maximum reactive power capability can help in increasing the linear modulation range.

Based on the comparison of the cases of whether or not taking into account the CVR effect shown in Fig. 8, the conventional method, which does not take into account the CVR effect, will yield a lower linear modulation range, which is inaccurate and results in higher arm current, loss, and SM capacitance. An accurate linear modulation range may be obtained by taking

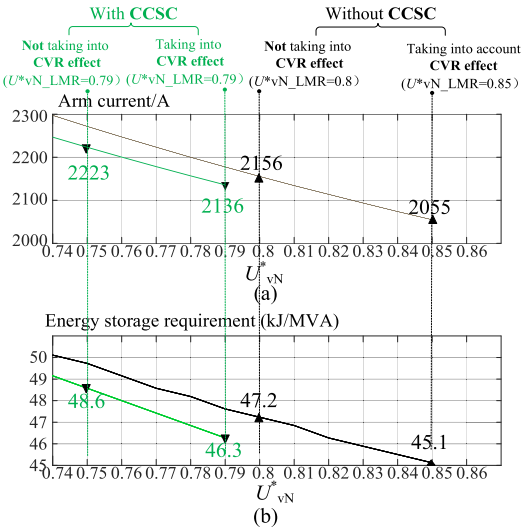

Fig. 9. Comparison results for various cases when $Q_{\max} = 1.0$ p.u.: (a) arm current (rms) and (b) energy storage requirement.

into account the CVR effect, thereby reducing the arm current, loss, and SM capacitance.

According to the comparison of the curves of whether the CCSC is active or not, as shown in Fig. 8, CCSC decreases the linear modulation range, which is consistent with the above presented analysis. When evaluating the effects of CCSC on the MMC parameters and operating characteristics, its impacts on the linear modulation range should be taken into account, which will be analyzed in detail in the following section.

C. Effect Analysis of the Linear Modulation Range on the Parameter Design and Operating Characteristics

In a given rated power, the higher the valve-side voltage U^*_{vN}, the lower the arm current, loss, and SM capacitance. This section demonstrates how the CVR effect and CCSC influence the converter parameter design and operating characteristics from the view point of linear modulation range using the case study shown in Table I. The normalized energy storage E_{nom}, which is defined in Appendix, is used to indicate the total SM capacitance usage of an MMC. When determining the energy storage requirement in the case study, the upper limit of the capacitor voltage peak is set as 1.1 p.u.

Fig. 9 depicts the curves of the arm current and normalized energy storage requirement varying with U^*_{vN} when $Q_{\max} = 1.0$ p.u. First, the case without CCSC is analyzed. The linear modulation range $U^*_{\mathrm{vN\_LMR}}$ is judged as only 0.8 p.u when using the conventional method that does not take into account the CVR effect. However, this result is an underestimated value. When taking into account the CVR effect, $U^*_{\mathrm{vN\_LMR}}$ can actually reach 0.85 p.u. Specifically, the valve-side voltage can be increased by 6.3% when considering the CVR effect in this example. Accordingly, the rated rms arm current can be decreased from 2156 to 2055 A (i.e., a 4.7% reduction), as illustrated in Fig. 9(a). This notion means a corresponding reduction of the current stress and power loss when taking into account the CVR effect.

Furthermore, the energy storage requirement E_{nom} also decreases with the increase in the valve-side voltage. This is partly due to the decreased arm current caused by the increased valve-side voltage. Another reason is that increasing the modulation index also directly decreases the energy variation in the arm according to the nonlinear relationship between them, which have been well reported in existing literature [12]. In Fig. 9, when the CVR effect is not taken into account, the linear modulation range is underestimated as 0.8 p.u. and the calculated result of E_{nom} is 47.2 kJ/MVA. However, the valve-side voltage can be properly selected as 0.85 p.u. when using the proposed methodology that takes into account the CVR effect. Thus, the energy storage requirement E_{nom} can be decreased from 47.2 to 45.1 kJ/MVA (i.e., a 4.4% reduction), as shown in Fig. 9(b).

The influence of the CCSC on the MMC parameter design and operating characteristics is also reconsidered in this article. The application of CCSC can help in reducing the arm current and energy storage requirement because it can eliminate the second-harmonic component in the arm current and reduce the energy variation in the arm. This conclusion is true under the premise that the employed values of U^*_{vN} are the same when applying and not applying CCSC. However, the application of CCSC will result in the reduction of the linear modulation range. Accordingly, the maximum selectable values of U^*_{vN} for the cases with and without CCSC are different. In Fig. 9, the linear modulation range $U^*_{\mathrm{vN\_LMR}}$ is 0.85 p.u., and the corresponding rated arm current and energy storage requirement are 2055 A and 45.1 kJ/MVA, respectively, when the CCSC is not applied. When the CCSC is applied, the linear modulation range $U^*_{\mathrm{vN\_LMR}}$ is only 0.79 p.u., and the corresponding rated arm current and ESR are 2136 A and 46.3 kJ/MVA, respectively, which are even slightly higher than those when the CCSC is inactive. This finding is different from the conventional understanding about the effect of CCSC on the arm current and energy storage requirement because the influence of the CCSC on the linear modulation range is not considered in the conventional methodology. This finding indicates that the effect of CSCC should be reconsidered from the viewpoint of linear modulation range.

An example case of $Q_{\max} = 0.5$ p.u. is also studied, and the results are shown in Fig. 10. The main conclusions of the influence of the CVR effect and CCSC on the linear modulation range and the arm current and energy storage requirement are similar to those shown in Fig. 9. As shown in Fig. 10, when the CCSC is applied, the arm current and energy storage requirement are lower than those when the CCSC is inactive for the case of $Q_{\max} = 0.5$ p.u. However, the decline is still not as significant as estimated using the conventional methodology that does not take into account the influence of the CCSC on the linear modulation range.

V. Simulation and Experiment

A. Simulation Results

The simulation model of an MMC system is established using MATLAB/Simulink. The key parameters of the simulated MMC are listed in Table I. In the simulation, the MMC operates under active and reactive power control modes, and the dc voltage is

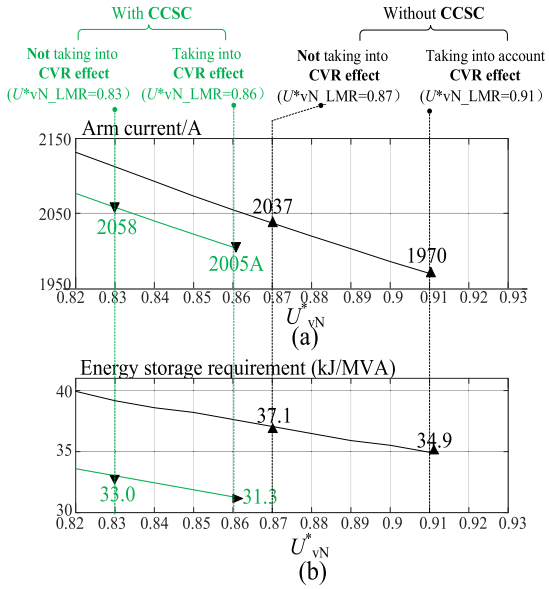

Fig. 10. Comparison results for various cases when $Q_{\max} = 0.5$ p.u.: (a) arm current (rms) and (b) energy storage requirement.

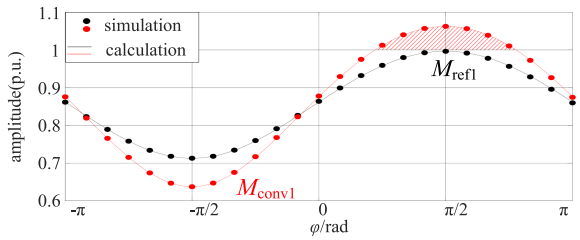

Fig. 11. Comparison of the simulated and theoretical results for the amplitudes of the actual AC voltage output and reference following the change of operating points along the boundary of the PQ diagram ($Q_{\max} = 1.0$ p.u., without CCSC).

kept as its rated value of 400 kV. The PQ diagram of the MMC is shown as Fig. 4, where $Q_{\max}$ is set as1.0 p.u.

In the case without CCSC, the valve-side voltage U^*_{vN} is set as $U^*_{\text{vN\_LMR}} = 0.85$ p.u., and the normalized energy storage is designed as $E_{\text{nom}} = 45.1$ kJ/MVA ($C_{\text{d}} = 23.5$ mF) in accordance with Fig. 9. The simulated results for various operating points are compared with the corresponding theoretical results to verify the correctness of the analytical model. In the simulation, the operating points for the φ-varying step by $\pi/12$ along the boundary of the PQ diagram are simulated. The simulated and analytically calculated amplitude of the fundamental-frequency reference wave varying with operating points are illustrated in Fig. 11. The comparison results have shown that the theoretical and simulated results fit well.

The linear modulation condition is more critical in the capacitive operating region, especially at the rated capacitive reactive power point, because the MMC is required to generate a higher ac voltage when outputting capacitive reactive power. The results shown in Fig. 11 also verify that the CVR effect plays a role in increasing the ac voltage output capability in the capacitive operating range. Although the actual ac voltage amplitude is larger than 1.0 in the shadowed area, the reference amplitude is still below 1.0, and the MMC is actually still in a linear modulation status due to the CVR effect. If the CVR effect is not taken into account and the reference voltage is simply considered the same with the actual ac voltage output, then it will be misjudged that overmodulation occurs in the shadowed area. Therefore, taking into account the CVR effect can help in fully utilizing the ac voltage output capability, which is underestimated in the conventional methodology without considering the CVR effect.

Fig. 12 illustrates the detailed waveforms of the simulation for several typical operating conditions when the CCSC is inactive. First, obvious deviations can be observed between the waveforms of the actual ac voltage output u^*_{conv1} and the reference u^*_{ref1}. At the active power operating conditions, such as $\varphi = 0$ and $\varphi = -\pi$, the deviation is mainly reflected in the phase difference, and the amplitude difference is minor. At the reactive power operating conditions, such as $\varphi = -\pi/2$ and $\varphi = \pi/2$, the deviation is mainly reflected in the amplitude difference and affects linear modulation. Although the amplitude of the ac voltage output is beyond 1.0 p.u. when the MMC is required to output the rated capacitive reactive power, the reference amplitude is still below 1.0 p.u., and the linear modulation condition is still satisfied, as illustrated in Fig. 12(d). This finding verifies that the CVR effect can improve the ac voltage output capability at capacitive reactive operating conditions.

Fig. 13 illustrates the detailed waveforms of the simulation for several typical operating conditions when the CCSC is activated. In this case, the valve-side voltage U^*_{vN} is set as $U^*_{\text{vN\_LMR}} = 0.79$ p.u., and the energy storage is designed as $E_{\text{nom}} = 46.3$ kJ/MVA ($C_{\text{d}} = 24.1$ mF) in accordance with Fig. 9. The simulation results show that the MMC with CCSC has similar CVR effects with that in the case without CCSC. Besides the CVR effects, the generated second-harmonic reference component also affects the peak and valley values of the reference wave function and the linear modulation condition. In Fig. 13(d), the peak and valley of the fundamental-frequency reference correspond with the valley of the second-harmonic reference at the rated capacitive reactive power point ($\varphi = \pi/2$). Thus, f_{valley} becomes closer to the lower limit and reduces the linear modulation margin.

B. Experimental Results

An MMC prototype was built to verify the proposed theory. The ac-side of the MMC was connected to a four-quadrant regenerative ac power source, and the dc-side of the MMC was connected to a programmable bidirectional dc power supply. The main parameters of the prototype are listed in Table II. The main component parameters are not changed with the operating modes because the component parameters of the MMC prototype cannot be flexibly adjusted once the MMC prototype is built. All the experiments were conducted under the same SM capacitance and valve-side ac voltage. This section focuses on whether the experimental results are consistent with the theoretical analysis. Experiments for the various operating conditions have been performed, and the experimental results are consistent with the theoretical analysis. The experimental results when outputting the rated capacitive reactive power and active power are selected

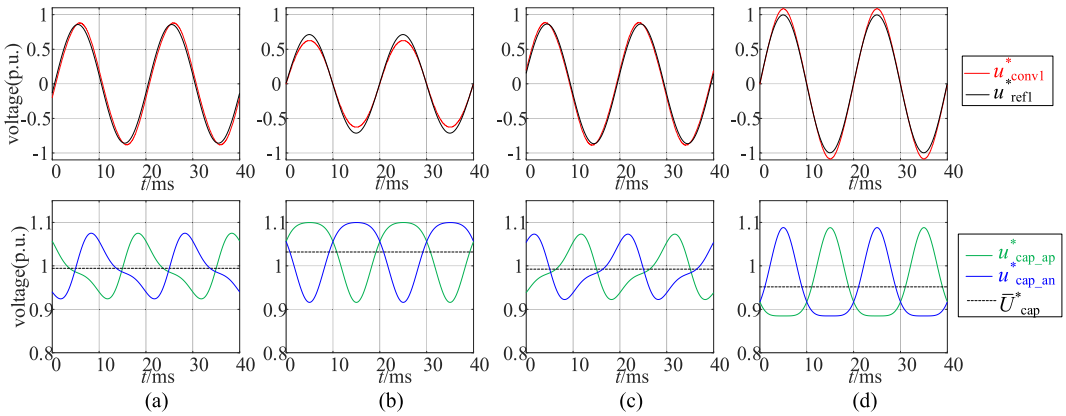

Fig. 12. Simulated waveforms for several typical operating conditions when CCSC is not applied ($U^*_{vN} = 0.85$, $Q_{max} = 1.0$ p.u.). (a) $\varphi = -\pi$. (b) $\varphi = -\pi/2$. (c) $\varphi = 0$. (d) $\varphi = \pi/2$.

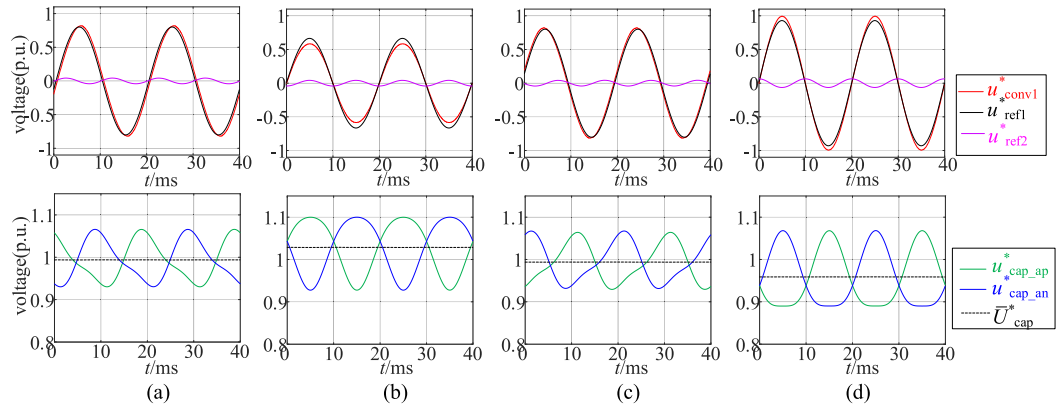

Fig. 13. Simulated waveforms for several typical operating conditions when CCSC is applied ($U^*_{vN} = 0.79$, $Q_{max} = 1.0$ p.u.). (a) $\varphi = -\pi$. (b) $\varphi = -\pi/2$. (c) $\varphi = 0$. (d) $\varphi = \pi/2$.

TABLE II
KEY PARAMETERS OF THE EXPERIMENTAL SETUP

Item	Value
Rated active power P	4000 W
Rated dc-link voltage U_{dcN}	300 V
Rated ac voltage U_{vN}	90 V
Number of SMs in an arm N	4
Rated SM capacitor voltage U_{capN}	75 V
Arm inductor L_{arm}	9 mH
SM capacitance C_d	1.17 mF

to be illustrated in Figs. 14–17 due to the page limitation. The waveform of the fundamental-frequency ac voltage u_{conv1} is extracted from the measured waveform of the ac voltage output because the number of levels of the MMC prototype is low, and the ac voltage output still contains considerable high-frequency harmonics.

Figs. 14 and 15 illustrate the experimental waveforms when outputting a 4 kVar capacitive reactive power ($\varphi = \pi/2$) without and with CCSC, respectively. In Fig. 14(a), the amplitude of u_{conv1} is larger than that of u_{ref1} under capacitive reactive power operating condition, which is consistent with the theoretical analysis and the simulation results. In this experiment, the amplitude of u_{conv1} is already higher than 150 V (i.e., $U_{dcN}/2$), indicating that M_{conv1} has exceeded 1.0. However, the peak and valley values of the reference wave function $f_{ref}(t)$ are still within the upper and lower boundaries due to the CVR effect, as illustrated in Fig. 14(c), and linear modulation is still satisfied. Specifically, if the CVR effect is not taken into account, then valve-side voltage U_{vN} cannot be selected as high as that in this experiment.

Fig. 15 shows the results when CCSC is applied. In Fig. 15(a), the phenomenon of the deviation between the actual ac voltage output u_{conv1} and the reference u_{ref1} is similar to that when CCSC is inactive. In Fig. 15(b), the second-harmonic circulating component is eliminated from the arm currents. However, the second-harmonic reference generated by the CCSC distorts the waveform of the reference wave function $f_{ref}(t)$ and decreases the valley value of $f_{ref}(t)$, as illustrated in Fig. 15(c). Fig. 15(c) demonstrates that the valley value of $f_{ref}(t)$ has decreased below zero, which is the lower boundary of linear modulation for an HB-MMC. Specifically, overmodulation already occurred in this experiment for an HB-MMC. This phenomenon indicates that the valve-side ac voltage for the case with CCSC cannot be designed as high as that in the case without CCSC. However, if the valve-side voltage is decreased, then the arm current will

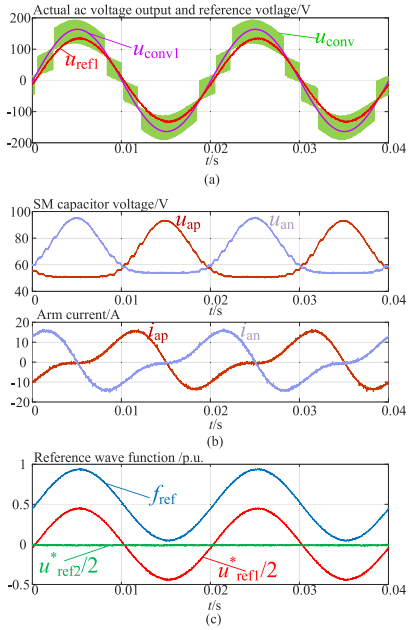

Fig. 14. Experimental waveform of capacitive mode without CCSC.

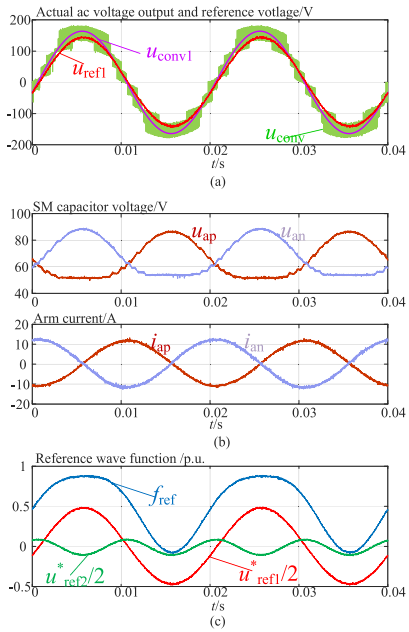

Fig. 15. Experimental waveform of capacitive mode with CCSC.

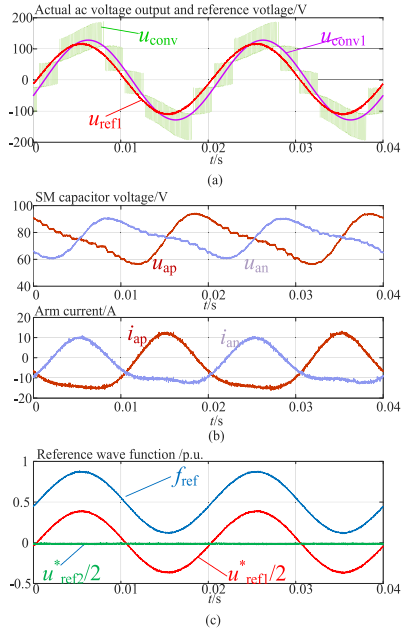

Fig. 16. Experimental waveform of the rectifier mode without CCSC.

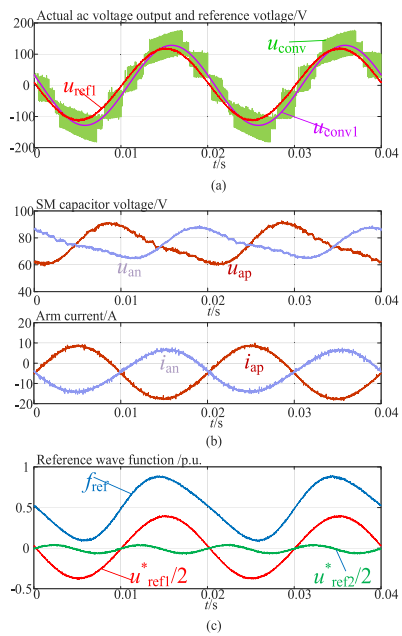

Fig. 17. Experimental waveform of the rectifier mode with CCSC.

increase, resulting in the increase in the loss and energy variation in the arm. This experimental phenomenon is consistent to the theoretical analysis.

Figs. 16 and 17 illustrate the experimental waveforms when the MMC absorbs an active power of 4 kW ($\varphi = -\pi$) without and with CCSC. The CVR effect is mainly reflected in the phase difference between the actual ac voltage output u_{conv1} and the reference u_{ref1}. The second-harmonic reference also has a minor influence on the peak and valley values of the reference wave function because the zero points of the second-harmonic reference correspond to the peak and valley points of the fundamental-frequency reference under active power operating condition. Therefore, the CVR effect and CCSC have a minor influence on linear modulation under active power operating condition, which is consistent with the theoretical result.

VI. Conclusion

In this article, the linear modulation range of MMC and its influence on the parameter design and operating characteristics are reconsidered by taking into account the CVR effect and CCSC. The CVRs cause the deviation between the amplitudes

of the reference wave and the actual ac voltage output and affect linear modulation. Although the deviation degree varies with the operating conditions, the linear modulation range must be increased because the CVR effect plays a role in increasing the actual ac voltage output under capacitive operating conditions, under which the required ac voltage amplitude is higher. Furthermore, the second-harmonic reference generated by the CCSC is unfavorable to linear modulation because it distorts the reference wave and makes the peak and valley value of the reference closer to the upper or lower boundary of linear modulation. Based on the analysis, a set of 4-D equations are determined to solve the exact reference wave taking into account the CVR effect and CCSC, which provides an effective way to exactly judge the linear modulation for any given operating point. Given that the parameter design should consider WOR-LM, this article proposes to define the linear modulation range of MMC using the maximum selectable valve-side voltage that can satisfy WOR-LM. The methodology for exactly determining the linear modulation range of MMC is also proposed. The analysis for the case studies shows that the exact linear modulation range can be obtained by taking into account the CVR effect, which is underestimated in the conventional methodology that does not take such an effect into account. Accordingly, the arm current, loss, and energy storage requirement can be reduced when taking into account the CVR effect compared with the conventional methodology. The analysis results also show that the CCSC will reduce the linear modulation range. Although the CCSC can eliminate the second-harmonic component in the arm current, the fundamental-frequency arm current will be increased because the maximum selectable valve-side ac voltage is decreased. Therefore, the effect of CCSC on reducing the arm current, loss, and energy storage requirements may not be so strong as that conventionally believed. The proposed theory and method are verified using simulation and experimental results.

APPENDIX

The coefficient c_1 is calculated as follows:

$$c_1 = \frac{1}{8U^*_{\mathrm{vN}}\omega E_{\mathrm{nom}}} \tag{A1}$$

and E_{nom} is the normalized nominal energy storage expressed as follows:

$$E_{\mathrm{nom}} = \frac{\frac{1}{2}C_{\mathrm{d}}U^2_{\mathrm{capN}} \times N \times 6}{S_{\mathrm{N}}}. \tag{A2}$$

According to the steady-state model in [15], if the CCSC is inactive ($M_{\mathrm{ref2}} = 0$), then the amplitude and phase of the second-harmonic circulating current can be expressed as follows:

$$k_{\mathrm{cir}} = \frac{M_{\mathrm{ref1}}\sqrt{\cos^2(\varphi+\delta_{\mathrm{ref1}})\left(3-M^2_{\mathrm{ref1}}\right)^2 + \left[3\sin(\varphi+\delta_{\mathrm{ref1}})\right]^2}}{\frac{X^*_{\mathrm{arm}}U^*_{\mathrm{vN}}}{c_1} - 4 - \frac{8M^2_{\mathrm{ref1}}}{3}} \tag{A3}$$

$$\theta_{\mathrm{cir}} = \arctan \times \left[\cos(\varphi+\delta_{\mathrm{ref1}})\left(3-M^2_{\mathrm{ref1}}\right), 3\sin(\varphi+\delta_{\mathrm{ref1}})\right] + 2\delta_{\mathrm{ref1}}. \tag{A4}$$

REFERENCES

[1] A. Lesnicar and R. Marquardt, "An innovative modular multilevel converter topology suitable for a wide power range," in *Proc. IEEE Bologna Power Tech. Conf. Proc.*, Bologna, Italy, vol. 3, 2003, pp. 6, doi: 10.1109/PTC.2003.1304403.

[2] A. Nami, J. Q. Liang, F. Dijkhuizen, and G. D. Demetriades, "Modular multilevel converters for HVDC applications: Review on converter cells and functionalities," *IEEE Trans. Power Electron.*, vol. 30, no. 1, pp. 18–36, Jan. 2015.

[3] M. A. Perez, S. Bernet, J. Rodriguez, S. Kouro, and R. Lizana, "Circuit topologies, modeling, control schemes, and applications of modular multilevel converters," *IEEE Trans. Power Electron.*, vol. 30, no. 1, pp. 4–17, Jan. 2015.

[4] S. P. Teeuwsen, "Modeling the trans bay cable project as voltage-sourced converter with modular multilevel converter design," in *Proc. IEEE Power Energy Soc. Gen. Meeting*, 2011, pp. 1–8.

[5] S. Debnath, J. C. Qin, B. Bahrani, M. Saeedifard, and P. Barbosa, "Operation, control, and applications of the modular multilevel converter: A review," *IEEE Trans. Power Electron.*, vol. 30, no. 1, pp. 37–53, Jan. 2015.

[6] T. An, G. Tang, and W. Wang, "Research and application on multi-terminal and DC grids based on VSC-HVDC technology in China," *High Voltage*, vol. 2, no. 1, pp. 1–10, 2017.

[7] Q. Song, W. Liu, X. Li, H. Rao, S. Xu, and L. Li, "A steady-state analysis method for a modular multilevel converter," *IEEE Trans. Power Electron.*, vol. 28, no. 8, pp. 3702–3713, Aug. 2013.

[8] K. Ilves, S. Norrga, L. Harnefors, and H.-P. Nee, "On energy storage requirements in modular multilevel converters," *IEEE Trans. Power Electron.*, vol. 29, no. 1, pp. 77–88, Jan. 2014.

[9] Y. Tang, M. J. Chen, and L. Ran, "A compact MMC submodule structure with reduced capacitor size using the stacked switched capacitor architecture," *IEEE Trans. Power Electron.*, vol. 31, no. 10, pp. 6920–6936, Oct. 2016.

[10] C. Zhao, Z. Wang, Z. Li, P. Wang, and Y. Li, "Characteristics analysis of capacitor voltage ripples and dimensioning of full-bridge MMC with zero sequence voltage injection," *IEEE J. Emerg. Sel. Topics Power Electron.*, vol. 7, no. 3, pp. 2106–2115, Sep. 2019.

[11] J. Hu, M. Xiang, L. Lin, M. Lu, J. Zhu, and Z. He, "Improved design and control of FBSM MMC with boosted AC voltage and reduced DC capacitance," *IEEE Trans. Ind. Electron.*, vol. 65, no. 3, pp. 1919–1930, Mar. 2018.

[12] Q. Song, W. B. Yang, B. Zhao, S. Xu, H. Rao, and Z. Zhu, "Energy storage requirement reduction using negative-voltage states of a full-bridge modular multilevel converter," *IEEE Trans. Power Electron.*, vol. 34, no. 6, pp. 5243–5255, Jun. 2019.

[13] Q. Tu, Z. Xu, and L. Xu, "Reduced switching-frequency modulation and circulating current suppression for modular multilevel converters," *IEEE Trans. Power Del.*, vol. 26, no. 3, pp. 2009–2017, Jul. 2011.

[14] B. Bahrani, S. Debnath, and M. Saeedifard, "Circulating current suppression of the modular multilevel converter in a double-frequency rotating reference frame," *IEEE Trans. Power Electron.*, vol. 31, no. 1, pp. 783–792, Jan. 2016.

[15] X. Li, Q. Song, W. Liu, S. Xu, Z. Zhu, and X. Li, "Performance analysis and optimization of circulating current control for modular multilevel converter," *IEEE Trans. Ind. Electron.*, vol. 63, no. 2, pp. 716–727, Feb. 2016.

[16] S. Kolluri, N. B. Y. Gorla, and S. K. Panda, "Capacitor voltage ripple suppression in a modular multilevel converter using frequency-adaptive spatial repetitive-based circulating current controller," *IEEE Trans. Power Electron.*, vol. 35, no. 9, pp. 9839–9849, Sep. 2020.

[17] H. Yang, Y. Dong, W. Li, and X. He, "Average-value model of modular multilevel converters considering capacitor voltage ripple," *IEEE Trans. Power Del.*, vol. 32, no. 2, pp. 723–732, Apr. 2017.

[18] Y. Ma, H. Lin, and Z. Wang, "Equivalent model of modular multilevel converter considering capacitor voltage ripples," *IEEE Trans. Power Del.*, vol. 34, no. 6, pp. 2182–2193, Dec. 2019.

[19] C. Oates, "Modular multilevel converter design for VSC HVDC applications," *IEEE J. Emerg. Sel. Topics Power Electron.*, vol. 3, no. 2, pp. 505–515, Jun. 2015.

[20] Z. Liu, K.-J. Li, J. Wang, Z. Javid, M. Wang, and K. Sun, "Research on capacitance selection for modular multi-level converter," *IEEE Trans. Power Electron.*, vol. 34, no. 9, pp. 8417–8434, Sep. 2019.
[21] Q. Song, W. Yang, B. Zhao, J. Meng, S. Xu, and Z. Zhu, "Low-capacitance modular multilevel converter operating with high capacitor voltage ripples," *IEEE Trans. Ind. Electron.*, vol. 66, no. 10, pp. 7456–7467, Oct. 2019.
[22] J. Wang and P. Wang, "Decoupled power control for direct-modulation-based modular multilevel converter with improved stability," *IEEE Trans. Ind. Electron.*, vol. 66, no. 7, pp. 5264–5274, Jul. 2019.
[23] K. Ilves, A. Antonopoulos, S. Norrga, and H.-P. Nee, "Steady-state analysis of interaction between harmonic components of arm and line quantities of modular multilevel converters," *IEEE Trans. Ind. Electron.*, vol. 27, no. 1, pp. 57–68, Jan. 2012.
[24] Ö. C. Sakinci and J. Beerten, "Equivalent multiple dq-frame model of the MMC using dynamic phasor theory in the $\alpha\beta$z-Frame," *IEEE Trans. Power Del.*, vol. 35, no. 6, pp. 2916–2927, Dec. 2020.

Jingwei Meng was born in Liaoning, China, in 1990. He received the B.S. degree in electrical engineering from the Department of Electrical Engineering, Tianjin University, Tianjin, China, in 2015, and the M.S. degree in electrical engineering from the Department of Electrical Engineering, Tsinghua University, Beijing, China, in 2018. He is currently working toward the Ph.D. degree in electrical engineering with the Tsinghua University, Beijing, China.

His research interest includes voltage-source converter HVdc system.

Qiang Song (Senior Member, IEEE) was born in Changchun, China, in 1975. He received the B.E.E. and Ph.D. degrees in electrical engineering from the Tsinghua University, Beijing, China, in 1998 and 2003, respectively.

From 2003 to 2008, he was a Lecturer with the Department of Electrical Engineering, Tsinghua University. Since 2008, he has been an Associate Professor with the Department of Electrical Engineering, Tsinghua University. His research interests include high-power electronic interfaces for utility system, flexible ac transmission system, VSC-HVdc system, and custom power quality.

Qianhao Sun was born in Shanxi, China, in 1993. He received the B.S. degree in electrical engineering from the Northeast Electric Power University, Jilin, China, in 2014, and the M.S. and Ph.D. degrees in electrical engineering from the Tsinghua University, Beijing, China, in 2017 and 2020, respectively,

He is currently a Postdoctoral Fellow with the Tsinghua University. From May to November, 2019, he was a Visiting Ph.D. Student with the Cardiff University, Cardiff, U.K. His research interests include flexible ac and dc transmission and distribution system, renewable energy generation, high-power electronic interfaces for utility system, and dc–dc converter.

Shukai Xu (Senior Member, IEEE) received the B.E. and Ph.D. degrees in electrical engineering from the Tsinghua University, Beijing, China, in 2002 and 2007, respectively.

He is currently the Deputy Director with the Innovation Department of China Southern Power Grid. His research interests include FACTS and VSC-HVdc.

Biao Zhao (Senior Member, IEEE) was born in Hubei, China, in 1987. He received the B.S. degree in electrical engineering from the Department of Electrical Engineering, Dalian University of Technology, Dalian, China, in 2009, and the Ph.D. degree in electrical engineering form the Department of Electrical Engineering, Tsinghua University, Beijing, China, in 2014.

He is currently an Associate Professor with the Department of Electrical Engineering, Tsinghua University, Beijing, China. His research interests include high-power converter, high-power semiconductor device, and flexible dc transmission and distribution system.

Zhanqing Yu (Member, IEEE) was born in Inner Mongolia, China, in 1981. He received the B.Sc. and Ph.D. degrees in electrical engineering from the Department of Electrical Engineering, Tsinghua University, Beijing, China, in 2003 and 2008, respectively.

After graduation, he became a Postdoctor and Lecturer with the Department of Electrical Engineering, Tsinghua University, in July 2008 and July 2010, respectively, and an Associate Professor with the same department in December 2012. His research interests include dc grid, dc breaker, electromagnetic environment and electromagnetic compatibility, and lightning protection.

Rong Zeng (Senior Member, IEEE) was born in Shaanxi, China, in 1971. He received the B.E., M.E., and Ph.D. degrees in electrical engineering from the Department of Electrical Engineering, Tsinghua University, Beijing, China, in 1995, 1997, and 1999, respectively.

He was a Lecturer with the Department of Electrical Engineering, Tsinghua University, in 1999, and an Associate Professor and a Professor with the same department, in 2002 and 2007, respectively. His research interests include air gap discharge, lightning protection, and electromagnetic compatibility in power systems, electric and magnetic field measurement by integrated electro-optical sensors, power semiconductor, HVdc system, and direct current circuit breaker.